

Diethynylarene-linked bis(triarylborane)cations as theranostic agents for tumor cell and virus-targeted photodynamic therapy

Ksenija Božinović,[a], Davor Nestić,[a] Evripidis Michail,[d] Matthias Ferger,[c] Marta Koščak,[b] Christoph Lambert,[d] Dragomira Majhen,[a]* Todd B. Marder,[c]* Ivo Piantanida[b]*

[a] Division of Molecular Biology, Ruđer Bošković Institute, Zagreb, Croatia

[b] Division of Organic Chemistry & Biochemistry, Ruđer Bošković Institute, Zagreb, Croatia

[c] Institut für Anorganische Chemie, and Institute for Sustainable Chemistry & Catalysis with Boron, Julius-Maximilians-Universität Würzburg, Am Hubland, 97074 Würzburg, Germany

[d] Institut für Organische Chemie, Julius-Maximilians-Universität Würzburg, Am Hubland, 97074 Würzburg, Germany.

Abstract:

Recently prepared diethynylarene-linked bis(triarylborane) cations, reported to show remarkable fluorimetric and Raman-SERS sensing of DNA/RNA, in this study exhibited promising photodynamic therapy (PDT)-based biological activity on human cell lines and adenovirus type 5 (HAdV5), acting as theranostic agents. All compounds efficiently enter living cells showing negligible antiproliferative activity. Bis-thiophene- and anthracene-analogues bind non-covalently to HAdV5 virus with high affinity, the anthracene-analogue itself causing a moderate antiviral effect, i.e. decreased ability of the virus to infect human cells. The irradiation of bis-thiophene- and anthracene- analogues with visible light (400-700 nm) caused a very rapid (within 1 minute) and strong increase in cytotoxicity, as well as an order of magnitude increase in antiviral activity, attributed to the formation of reactive oxygen species (ROS). Photochemical studies of the compounds revealed that, upon irradiation, they produce singlet oxygen, which correlates with the observed light-induced bioactivity.

Keywords: bis(triarylborane) cations; singlet oxygen; photodynamic bioactivity; fluorescence; theranostics

1. Introduction

Photodynamic therapy (PDT) is one of the highly selective and thus attractive tools in the treatment of cancer, due to several advantages over the traditional treatment modalities, i.e., minimal invasiveness, negligible cytotoxicity, high local selectivity to cancer cells, high controllability and consequently less severe side effects [1,2,3,4]. The mechanism of PDT is based on the accumulation of the non-toxic compound (photosensitizer, PS [5]) within the well-defined solid tumor tissue, which is then locally excited by visible or near infra-red (NIR) light, inciting the PS to produce strongly cytotoxic species and consequently leading to cell death, highly selectively within the irradiated part of the body [2,6]. Originally developed as a tumor therapy, PDT has been also proven useful in treating non-malignant disorders [7,8].

Energy transfer from the PS to oxygen can induce formation of reactive oxygen species (ROS), or yield toxic singlet oxygen [2]. Clinical application of PDT has been hindered by the low penetration of visible light through biological tissue, making deeper tissue impossible to treat with this approach [9]. Therefore, new organic chromophores with the ability to absorb in NIR light in the therapeutic optical window for biological tissues (600–1300 nm) have been developed in order to circumvent limitations of penetration depth [10,11,12]. One way to achieve that is tailoring a non-toxic organic compound that absorbs visible light, but can be also excited in the near IR using a non-linear two photon absorption (2PA) approach [13,14]. In other words, the compound would be excited by simultaneous absorption of two photons of half the energy (twice the wavelength) required for one photon absorption. This allows chromophores that naturally absorb energy in visible region to be efficiently excited in the near IR (within therapeutic optical window), without harming the biological tissue. Small, non-toxic, fluorescent molecules that have the ability to bind to DNA/RNA/proteins would be ideal candidates as PS in PDT.

We have been interested in the linear and nonlinear optical properties of triarylboranes and their potential applications in cells for some time [15]. In a previous study, we prepared new luminescent tetracationic bis-triarylborane dyes characterized by diethynylarene linkers [16], which finely sensed the shape and secondary structure of ds-DNA/RNA by simultaneous fluorescence and Raman-SERS detection. Some of these novel molecules possess aromatic moieties known for their ability to induce singlet oxygen production upon irradiation with light (anthracene [17], oligothiophene [18]). Such a property makes these molecules potentially bioactive, not only in the ground state, but even more active in the excited state, caused by irradiation with a corresponding light source. This presumption was additionally corroborated by previously reported efficient cellular uptake of their close analogues [19,20,21,22], which accumulated within cytoplasmic organelles.

Therefore, in this study, we focused on compounds **3** (bithiophene) and **5** (anthracene), as well as presumably non-photoactive analogue **4** (phenylene) (Figure 1), and studied in detail their photophysical properties under irradiation (related to singlet oxygen production), by both one-photon and two-photon absorption (2PA). Furthermore, we assessed the cytotoxic properties of **3** and **5** toward normal human lung and cancer cell lines, both in the dark and under irradiation with visible light. By confocal fluorescence microscopy we studied their cellular uptake, intracellular distribution and light-induced damage to stained cells. As we previously reported that triarylborane-containing compounds non-covalently bind to protein [22,23] we assumed they could also interact with viral protein capsid or viral DNA/RNA, therefore herein we assessed the antiviral activity of compounds **3** and **5** against adenovirus type 5 (HAdV5) with or without visible radiation, aiming toward virus-targeted PDT.

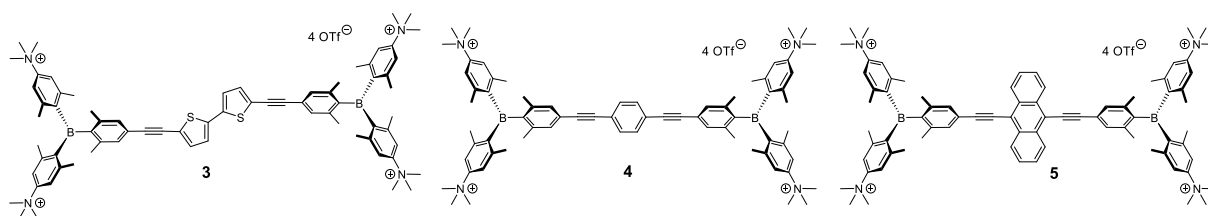


Figure 1. Structures of compounds **3**, **4**, and **5**.

Herein we present data regarding the photophysical, photochemical and biological properties of these compounds showing their high potential for application in theranostic tumor and antiviral strategies.

2. Materials and Methods

Photochemical study:

Detection of singlet oxygen luminescence. All measurements were performed in standard quartz cuvettes (1 cm x 1 cm cross-section) under ambient conditions, unless stated otherwise. UV-visible absorption spectra were recorded using an Agilent 8453 diode array UV-visible spectrophotometer. Emission spectra were recorded using an Edinburgh Instruments FLSP920 spectrometer equipped with a 450 W Xenon arc lamp, double monochromator for both excitation and emission, and a red-sensitive photomultiplier (PMT-R928P) and a near-IR PMT as detectors, operating in right-angle geometry mode, and all spectra were fully corrected for the spectral response of the instrument. All solutions used in photophysical measurements had concentrations lower than 5×10^{-6} M to minimize inner filter effects during luminescence measurements.

Two Photon Absorption (2PA). The 2PA cross-section, $\sigma^{(2PA)}$, of the chromophores was determined by the two-photon induced fluorescence technique (2PIF). It is based on

relative measurements with respect to a secondary reference standard with a well characterized 2PA spectrum and cross-section. A Ti: sapphire amplifier (Solstice, Spectra Physics) operating at 1 kHz, delivering 100 fs pulses at 800 nm served as the pulse source. 70 % of the available energy (2.5 mJ) seeds a tunable computer-controlled optical parametric amplifier (TOPAS-C, Light Conversion) which is used as the excitation source. A parabolic mirror with a 15 cm focal length was used in order to focus the vertically polarized light ca. 10 mm in front of the sample, while upon each acquisition the excitation energy was varied between 0.2-3 μ J. The emitted fluorescence signal was collected at 90° using an achromatic lens and then directed to a compact CCD spectrometer for detection. Coumarin 153 in methanol and fluorescein in aqueous alkaline solution were used as the secondary reference standards. [24,25] Maintenance of identical excitation conditions for reference and samples was achieved using a high precision motorized rotational stage. Two-photon excitation was verified by log-log plots of fluorescence intensities vs. excitation power at various wavelengths, all giving slopes of 2.

Cells. HEK293 (human embryonic kidney; ATCC CRL-1573), A549 (human lung carcinoma; ATCC CCL-185) and WI-38 (human normal lung fibroblast; ATCC CCL-75) were obtained from the ATCC Cell Biology Collection and were cultured according to the manufacturer's instructions. Cells were grown in Dulbecco Modified Eagle's Medium (DMEM, Sigma Aldrich, USA) supplemented with 10% of fetal bovine serum (FBS, Sigma Aldrich, USA) at 37 °C and 5% CO₂ in a humidified atmosphere. Three biological replicas were performed for all experiments.

Cytotoxicity assay – MTT. Studied compounds were dissolved in an appropriate volume of dimethyl sulfoxide solution (DMSO) under sterile conditions, in order to obtain 10 mM stock solutions and were kept in the dark at +4 °C. Prior to each assay, fresh working solutions were prepared from the stock solution by diluting them with DMEM. Cells were seeded on 96 well plates at concentrations of 7×10^3 cells/well in 100 μ L of DMEM (10% FBS) and left in the incubator overnight (37 °C, 5% CO₂). The next day, 100 μ L of the working solution was added to the wells, thus the final volume was 200 μ L/well. All measurements were made in quadruplicate. Cells treated with the same dilutions of DMSO represented the control, while cells treated only with DMEM (10% FBS) represented the negative control. The plate was then incubated for the next 72 h (37 °C, 5% CO₂). After incubation, the medium was removed, and 40 μ L of a MTT solution was added to each well. The plate was incubated in the cell incubator for 3 h, allowing formazan crystals to form. After 3 h, 170 μ L of DMSO was added to each well and the plate was placed on a shaker for 20 min, allowing the crystals to dissolve. The absorbance of the MTT-formazan product was measured with a microplate reader at 600 nm, and the absorbance value correlates directly with cell survival. For irradiation experiments, cell culture plates, prepared as above, were treated with the compounds studied, incubated for 90 min (37 °C, 5% CO₂) in order to allow the compounds to enter the cells, and

irradiated in a Luzchem reactor with visible light (400-700 nm, 8 lamps, in total 8 W, dose 50.6 mw m⁻², with a lamp to cell-plate distance of ca. 18 cm). Irradiation for 10 min, 30 min, and 1 h per day was performed on three consecutive days the same times

Detection of ROS. A549 cells were seeded in 12-well tissue culture plates (2 x 10⁵ cells/well). After 24 h, cells were treated with a 10 µM working solution of compounds **3** and **5** and incubated for 90 min (37 °C, 5% CO₂), allowing the compounds to enter the cells. Cells treated with the same dilution of DMSO represented the control sample. Cells were irradiated once for 30 min in a Luzchem reactor with visible light (400-700 nm, 8 lamps, in total 64 W, dose 50.6 mw m⁻², with a lamp to cell-plate distance of ca. 18 cm). One plate was irradiated with visible light (400-700 nm), the same as for the cytotoxicity assay, while non irradiated cells served as a control, and were incubated in the cell incubator (37 °C, 5% CO₂) during the whole experiment. Cells were then washed with PBS, trypsinized, re-suspended with cold PBS supplemented with 10% FBS and centrifuged for 5 min (RT, 1100 g). Cell pellets were re-suspended and washed again, but this time with cold PBS supplemented with 1% FBS and centrifuged for 5 min (RT, 1100 g). After the second washing, cell pellets were re-suspended in 5 µM 2',7'-dichlorofluorescein diacetate (H2DCFDA, Sigma, USA), which is converted to dichlorofluorescein (DCF) in contact with ROS, and incubated for 30 min (37 °C, 5% CO₂). Unstained cells were re-suspended in PBS supplemented with 1% FBS. Cells were then analyzed by flow cytometry (FACSCalibur, BD Biosciences, USA). The intensity of DCF fluorescence was analyzed in fluorescence channel 1 (FL-1), and morphology and integrity of cells was determined by analysing forward and side scatter of laser light, where forward scatter (FSC) gives information on the cell size, and side scatter (SSC) gives information on the cell granularity [26].

Co-localization Assay. A549 cells were seeded on glass slides in 24 well plate format at a concentration of 3 x 10⁴ cells/well. Cells were incubated in DMEM (37 °C, 5% CO₂) for 48 h, allowing cells to attach to the glass surface and multiply. Then, cells were treated with a 10 µM solution of the compound and incubated for 90 min on 37°C. After the incubation, cells were fixed with 2% paraformaldehyde (PFA, 12 min, RT), washed with PBS (3 times), permeabilized with 0.1% Triton X-100/PBS (2 min, RT), washed with PBS (3 times), blocked in 3% BSA (30 min, RT), and incubated with primary antibody against early endosome antigen 1 (EEA1, Cell Signalling Technology, #2411, rabbit, 1:100 in 5% BSA), Golgi Apparatus (GM130, Cell Signalling Technology, #12480, rabbit, 1:2500 in 5% BSA) or lysosome associated membrane protein 1 (LAMP-1, Abcam, ab2417, rabbit, 1:250 in 5% BSA). After incubation in primary antibodies, cells were washed with PBS, and then incubated in a fluorescently labelled anti-rabbit secondary antibody (AF647) (Cell Signalling Technology, #4414, 1:1000 in 5% BSA). Slides were incorporated in DAPI-containing mounting medium. Actin filaments were labelled with Alexa Fluor® 555 Phalloidin (Cell Signalling Technology, # 8953). The prepared slides were kept in the dark

and visualized using a Leica SP8 X confocal microscope (Leica Microsystems, Germany) with a 63 x/1.40 oil-immersion objective. Co-localization was assessed by the Pearson correlation coefficient. Analysis was done using ImageJ (NIH, USA) software and the appropriate JACoP plugin [27].

Live cell imaging. Live imaging of the cells treated with the compounds was performed on the A549 cell line. Cells were seeded in Ibidi imaging cell chambers (Ibidi®, Germany) in 500 μ L of medium, with a concentration of 5×10^4 cells/well, and left in the cell incubator for 48 h (37 °C, 5% CO₂). After two days, cells were treated with a 10 μ M solution of compound to be tested and left in the cell incubator for 90 min to allow compound to enter the cells. Then, the cells were rinsed and incubated with a 100 nM MitoTracker Deep Red solution (Invitrogen, Molecular Probes) in order to check for co-localization of compounds with mitochondria. The cells were incubated for 20 min at 37 °C, allowing the MitoTracker dye to enter the cells. After incubation, the medium was replaced with 500 μ L of fresh DMEM and the cells were immediately observed using the Leica SP8 X confocal microscope. Co-localization was assessed by the Pearson correlation coefficient. Analysis was done using ImageJ (NIH, USA) software and the appropriate JACoP plugin [27].

Interactions with human adenovirus type 5 (HAdV5):

Fluorimetric titrations with HAdV5 virus:

All experiments were performed on an Agilent Eclipse fluorimeter at 25 °C, pH = 7.0, Na cacodylate buffer, $I = 0.05$ M, in a 1 cm pathlength quartz cuvette, taking care of that the total absorbance of a sample at the excitation wavelength did not exceed 0.05. A stock solution of *HAdV5 virus* ($c_{\text{stock}}(\text{HAdV5}) = 2.90 \times 10^{12}$ vp ml⁻¹ (virus concentration calculated using the previously described method [28]) was added in small aliquots to the buffered solution of compounds **3** or **5** ($c = 5.0 \times 10^{-7}$ M) and, after each addition, the emission spectrum of **3** or **5** was measured (λ_{exc} (**3**) = 412 nm, λ_{exc} (**5**) = 470 nm). An incubation period of 2 min, after each addition, was sufficient for reaching fluorescence emission equilibrium. The binding affinity was estimated for compound **5** by assuming 1:1 binding stoichiometry of **5**/HAdV5 complex and fitting the titration data to the 1st exponential eq. in Origin 7.0.

End-point dilution assay: End Point Dilution Assay was used to determine the antiviral activity of compounds **3** and **5** against human adenovirus type 5 (HAdV5). HEK-293 cells were seeded in a 96 well plate at a concentration of 1×10^4 cells/well in 100 μ L of DMEM (10% FBS) and left in the incubator overnight (37 °C, 5% CO₂). The next day HAdV5 (2.9×10^9 viral particles) was incubated in culture medium (ctrl) or in a solution of the compounds (**3** and **5**, both 5×10^{-6} M) and illuminated using a 100 W light lamp for 10, 20

or 40 min, at a distance of ca. 10 cm from cell-plate. The control sample was illuminated for 40 min. After illumination, 3-fold serial dilutions of the virus in DMEM (10% FBS) were prepared and 100 μ L of the virus dilutions were added in octuplicates to HEK-293 with a starting dilution of 1×10^{-8} . After 10 days of incubation, all wells showing cytopathic affect (CPE) were counted using an inverted light microscope (Optika, Italy). Wells infected with the least dilute virus were all CPE-positive, while wells infected with the most dilute virus were all CPE-negative. Virus titer was calculated using the previously described method [28].

3. Results and Discussion

Reactivity of compounds **3**, **4**, and **5** with oxygen

The presence of singlet oxygen in solution can be verified by its luminescence at 1272 nm [29]. Upon excitation of O₂-saturated solutions of compounds **3**, **4**, and **5** (Figure 1) in MeCN, emission at 1272 nm was detected in each case (Figure 2). The respective quantum yields for singlet oxygen formation (Φ_{Δ}) are listed in Table 1 and were obtained by comparison to the standard perinaphthenone, which is known to sensitize singlet oxygen with an efficiency close to unity in MeCN [30]. A comparatively low radiative rate constant of 0.45 [31] for the luminescence of singlet oxygen at 1272 nm in MeCN explains the very low signal to noise ratio obtained. A measurement of singlet oxygen generation in water was not possible, as an even lower radiative rate constant of 0.16 [31] in water precluded detection of singlet oxygen luminescence with our experimental setup, even after sensitization by perinaphthenone. Importantly, the sum of the quantum yields for fluorescence (Φ_f) and singlet oxygen formation (Φ_{Δ}) is close to unity for compounds **3** and **5**, indicating their potential for PDT while simultaneously being able to observe their location via fluorescence. In addition, the high Φ_{Δ} for **3** is consistent with enhanced formation of the triplet state for this compound. Indeed, phosphorescence was observed at 77 K from a bis(4-tBu-phenylethynyl)thienylthiophene compound, also indicative of significant population of its triplet state [32].

Table 1. Fluorescence quantum yields (Φ_f) and quantum yields for singlet oxygen formation (Φ_{Δ}) in MeCN.

Compound	Φ_f	Φ_{Δ} ^{a)}
3	0.31	0.6
4	0.58	0.2
5	0.72	0.3

a) due to very low signal to noise ratio an error of ± 0.1 is assumed.

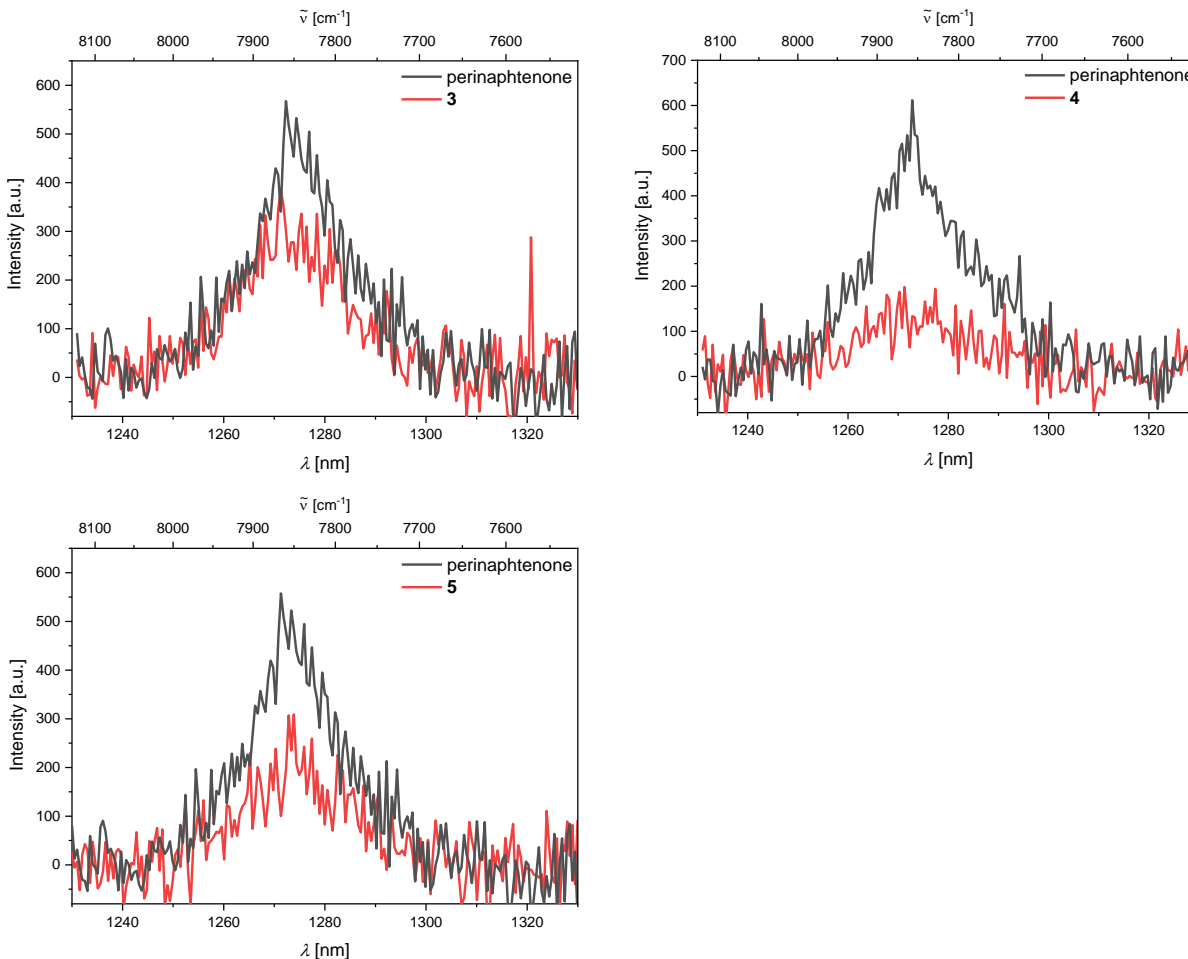


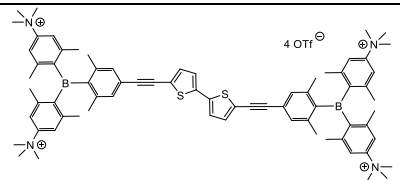
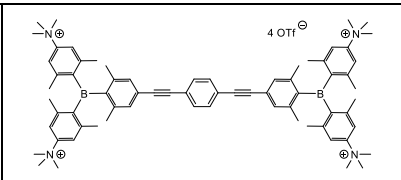
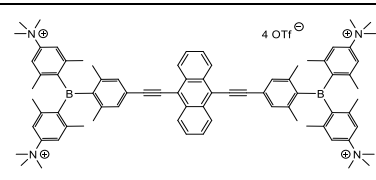
Figure 2. Emission spectra of singlet oxygen generated from sensitization by perinaphthenone in MeCN (black) compared to emission spectra of singlet oxygen generated by sensitization by compound **3** excited at 420 nm (top right), compound **4** excited at 388 nm (top left) and compound **5** excited at 420 nm (bottom left) in MeCN (red).

Two Photon Absorption (2PA) properties

When discussing good candidates for PDT, 2PA cross-section of the chromophores is of great importance, as well as singlet oxygen production yield. Most early photosensitizers had low 2PA cross-sections of about 50 Goeppert-Mayer (GM), which resulted in a low PDT efficiency under two-photon irradiation conditions [33,34,35], as the chromophore was not very efficiently excited via 2PA. In other words, singlet oxygen formation was not sufficient in order to induce tumor cell death. However, many studies reported significant 2PA cross-sections for highly π -conjugated small organic molecules applicable in PDT, some as high as 8000 GM [36,37], with metal-containing chromophores having even higher 2PA cross-sections[38], but mostly in the 100-1000 GM range [37,39,40,41].

However, some of those high 2PA values were accompanied with low singlet oxygen production yield, and other PS were of very high molecular weight, interfering with efficient drug uptake. Thus, ideal 2PA PDT candidate should balance between good 2PA cross-section (>100 GM), applicable singlet oxygen production yield (>0.1) and be of low molecular weight ($M_w < 700$). In that respect, some of our previously studied triarylborane cations revealed bio-applicable 2PA characteristics [21], therefore, prior to evaluation in a biological system, we measured the 2PA cross-sections of compounds **3-5**.

Table 2. 2PA cross-sections of compounds **3-5**.

		
Compound 3	Compound 4	Compound 5
350 GM at 770 nm	70 GM at 710 nm	390 GM at 770 nm

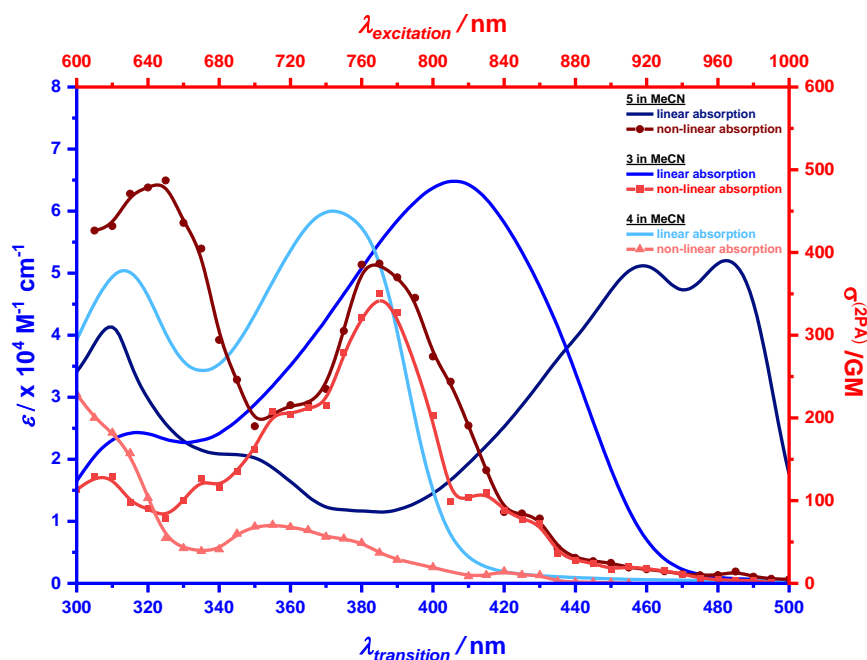


Figure 3. Linear (one photon) and non-linear (two photon) absorption spectra of compounds **3-5**

The 2PA spectra of both **3** and **5** in acetonitrile display strong, broad bands centered at 770 nm with similar 2PA cross-sections of 390 GM and 350 GM, respectively (Table 2, Figure 3). In contrast, the spectrum of **4** exhibits a considerably lower 2PA cross-section

of 70 GM at 710 nm. In the higher-energy region, several 2PA bands are visible for all compounds investigated, with compound **5** achieving a 2PA cross-section value of ca. 480 GM at ca. 645 nm.

Compounds **3** and **5** showed intriguing properties relevant for the photodynamic therapy, having rather efficient photo-induced singlet oxygen production yield and strong 2PA, which prompted us to study their biological activity in human cell lines.

Visible light irradiation increases cell toxicity and production of reactive oxygen species (ROS) by compounds 3 and 5.

In order to study the cytotoxic effect of compounds **3**, **4**, and **5**, human lung carcinoma (A549) and normal lung (WI-38) cell lines were treated with 10 μ M and 1 μ M solutions of the corresponding compounds, and cell survival was assessed by the MTT assay (Figure 4). The MTT assays for photoactive compounds **3** and **5** were performed in parallel: a) for non-irradiated cells (kept in the dark) and b) cells irradiated in a Luzchem reactor with visible light range. Irradiation was performed for three consecutive days at the same time point each day. Blank control experiments involving irradiation of non-treated cells demonstrated that light itself has no impact on cell survival rate. To determine whether the light-induced biological effect is proportional to exposure, the irradiation time was varied (10 min, 30 min, and 1 h per day).

With no exposure to light, all compounds tested show a slight cytotoxic effect on A549 and WI-38 cells at a concentration of 10 μ M, while at a 1 μ M concentration, none of the compounds tested had an influence on cell survival.

However, only 10 min/day irradiation of cells treated with the compounds resulted in a cytotoxic effect of compound **3** at both 10 μ M and 1 μ M concentrations, whereas photo-induced toxicity of compound **5** was measurable only at a 10 μ M concentration (Figure 4). Longer irradiation (up to 60 min) resulted in proportionally stronger cytotoxicity.

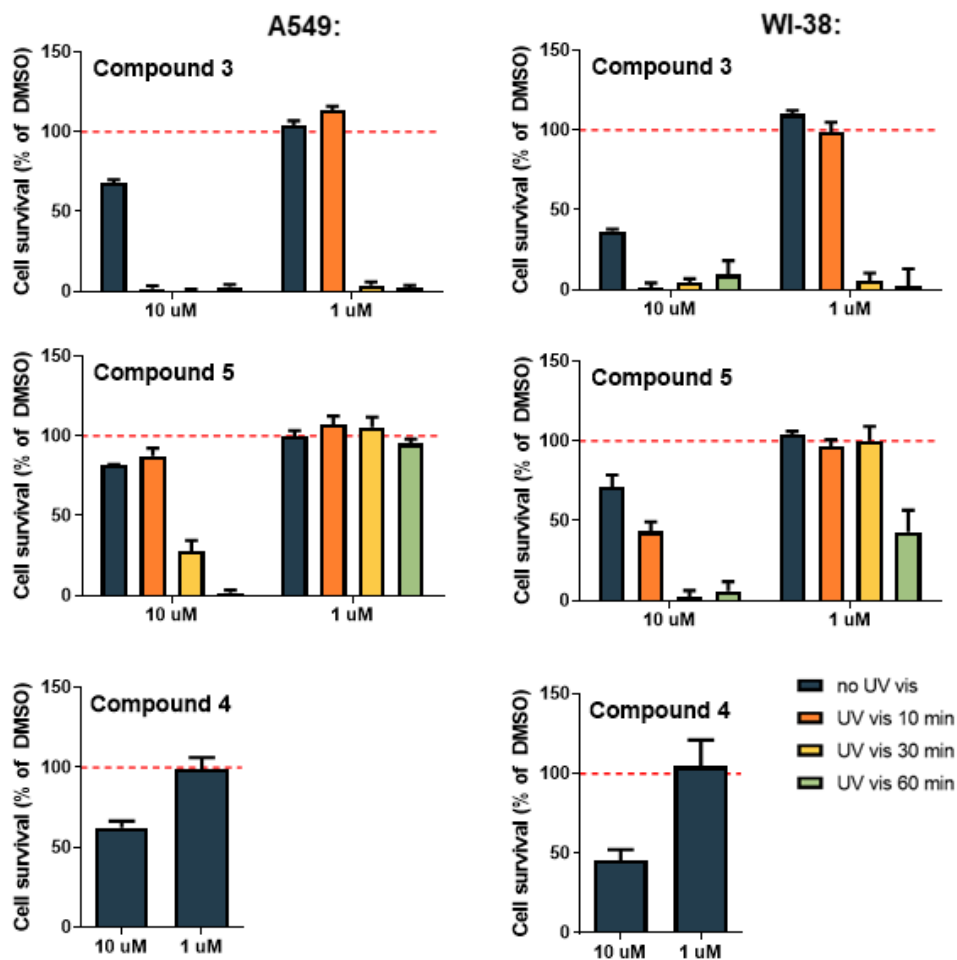


Figure 4. Cell survival of A549 and WI-38 cells treated with different concentrations of **3**, **4**, and **5**, with or without visible light irradiation. Data are presented as mean \pm SD made in four replicates, relative to the control samples. Control samples are cells treated with DMSO at the same concentration as the compound being tested. Representative data from three independent experiments which yielded similar results are shown.

We also performed irradiation experiments with **3** and **5** on a confocal microscope, using the maximum power laser irradiation at $\lambda_{exc} = 457$ nm, and monitoring the morphological changes of the irradiated cells in both bright-field and fluorescence ($\lambda_{em} = 500-600$ nm) modes. Compounds **3** and **5** efficiently entered treated cells after 90 min of incubation and mostly localized in cytoplasmic organelles (Fig. 6A, B), showing no particular effect if excited for about 5 min, by the laser source $\lambda_{exc} = 457$ nm at low power (10%). However, if the laser source power was increased to 100% (0.5 mW), cells treated with **3** or **5** showed strong morphological changes already after 1 min. irradiation, including severe blebbing and finally membrane disintegration (Supp. Info. Movie), effects which resemble typical ROS production and consequent cellular damage. Importantly, cells outside of the

laser focus circle were not affected; thus, photo-induced damage experiments could be repeated many times by simply shifting the laser focus over the same sample of living cells treated with **3** or **5**. In the control experiments, corresponding laser irradiation did not produce any observable effect on non-treated cells.

Due to the ability of the tested compounds to produce singlet oxygen species, exposing human cells to compounds **3** and **5** may result in an increased production of ROS. We, therefore, assessed the generation of ROS in A549 cells treated with 10 μM of the compounds, with or without exposure to visible light. As shown in Figure 5A, treating cells with compounds **3** and **5** induced production of intracellular ROS as indicated by fluorescence from DCF, which is shown by the shifted red curve in the histogram. The observed increase in ROS production was moderate for compound **3**, and high for compound **5**. Exposing A549 cells treated with compound **3** to visible light for 30 min caused changes in cell integrity (Figure 5B, yellow dot plot) compared to non-irradiated treated cells (red dot plot), namely decrease in cell size as evidenced by a decrease in the FSC signal. Under these conditions, we also observed two peaks indicating ROS production, one with higher and one with lower fluorescence intensity (yellow curve in histogram) indicating two cell population with different ROS production. As a majority of the cells lost membrane integrity, DCF dye was lost from them, resulting in the fluorescence peak being shifted to the left side of the histogram. Nevertheless, some cells retained cell integrity and no DCF dye was lost, hence, a small peak resembling cells with higher ROS production is also present.

We did not observe the same effect when we exposed cells to compound **5**. Moreover, compound **5** induced notably higher ROS production in cells, even without light exposure. In addition, irradiation of cells treated with compound **5** did not induce the same effect on cell integrity as in cells treated with compound **3**. Nevertheless, separation into two cell populations is visible; therefore, irradiation of cells treated with compound **5** induced changes in cell morphology, as seen in confocal microscopy experiment (Supp. Info., Movie).

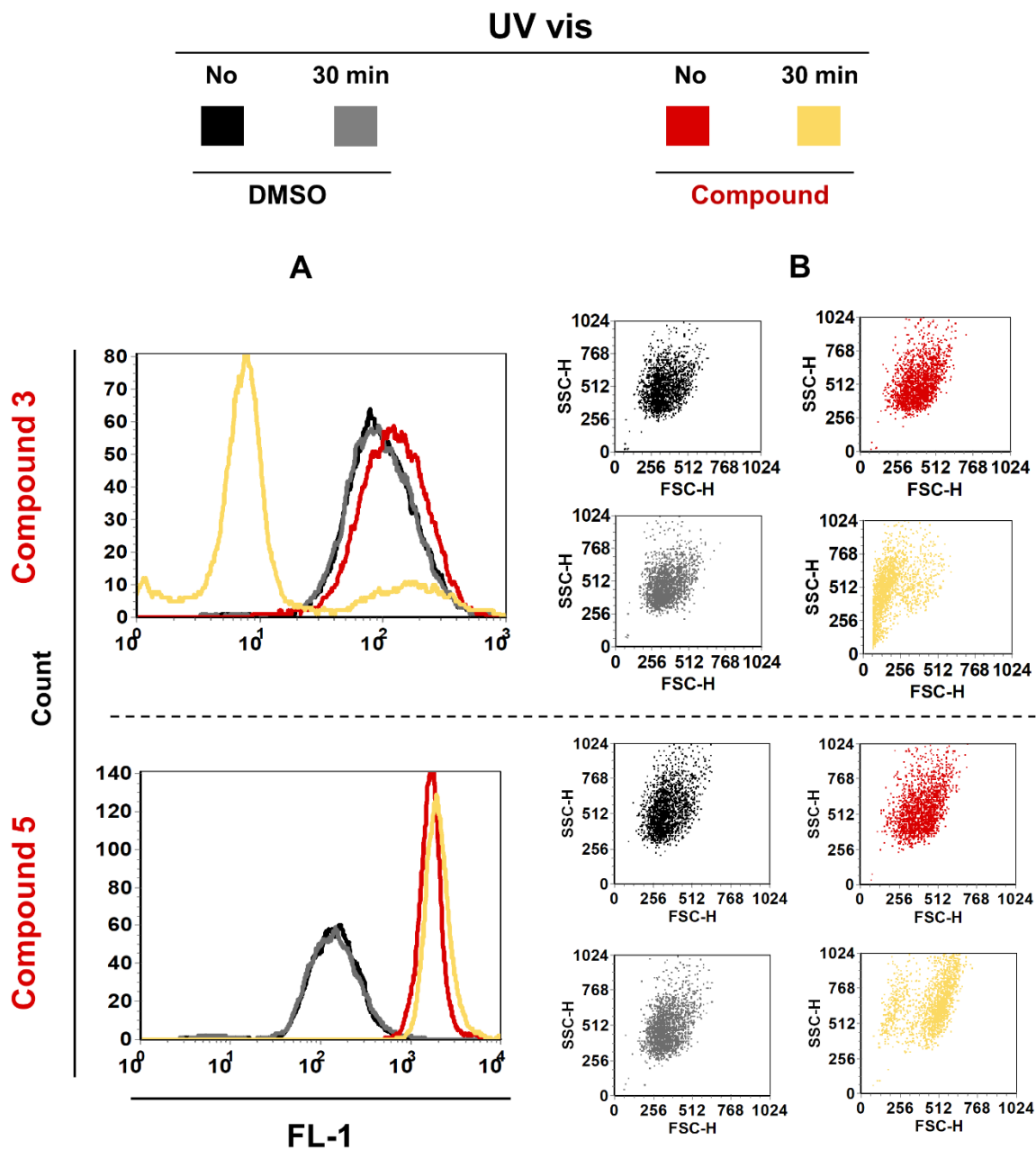


Figure 5. The amount of ROS (**A**) and cell morphology (**B**) of A549 cells treated with 10 μ M **3** or **5**, with or without exposure to visible light. Levels of ROS were assessed by measuring the fluorescence intensity of DCF by flow cytometry in fluorescence channel 1 (FL-1), and analysis of the cell population was visualized by two-parameter dot plots of forward (FSC) and side scatter (SSC) of laser light. Black and grey lines and dot plots represent control cells, i.e. cells treated with DMSO. Colored lines and dot plots represent cells treated with **3** or **5**. Representative data from two independent experiments which yielded similar results are shown.

Intracellular localization of compounds **3** and **5**

To investigate intracellular localization of compounds **3** and **5**, we performed colocalization experiments with stains specific for different cytoplasmic organelles: mitochondria, early endosomes, lysosomes, and Golgi, as these cell compartments have often been associated with different PDT compounds [2].

For assessing accumulation of **3** or **5** within mitochondria, we used MitoTracker Deep Red which is known to stain mitochondria in living cells. As shown in Figure 6, compounds **3** and **5** do not accumulate significantly in mitochondria (Pearson's coefficients are 0.16 and 0.18, respectively). Furthermore, we treated cells with **3** or **5**, fixed them with PFA and performed colocalization with EEA1 as a marker for early endosomes, LAMP1 as a marker for lysosomes and GM130 as a marker for Golgi. As can be seen in Figure 7, compound **3** shows partial but significant colocalization with GM130 (Pearson's coefficient 0.48) indicating that this compound partially accumulates in Golgi. Colocalization of **3** with EEA1 or LAMP1 was poor (Pearson's coefficient 0.19 and 0.28, respectively), suggesting that compound **3** negligibly accumulates within early endosomes or lysosomes. Compound **5** shows quite uniform, and thus non-selective, distribution over all studied intracellular compartments, i.e., early endosomes, lysosomes, Golgi and mitochondria (Figures 6,7).

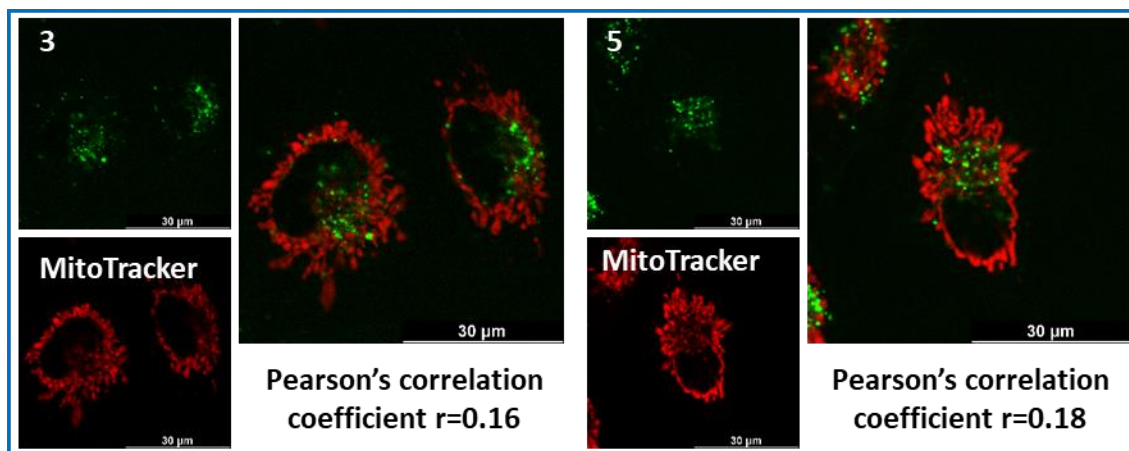


Figure 6. Colocalization of compounds **3** and **5** with mitochondria in live A549 cells. Colocalization of compounds (green) with “MitoTracker Deep Red” (red) observed by confocal microscopy. Cells were treated with 10 µM of compound **3** or **5** for 90 min at 37 °C and incubated with 100 nM “MitoTracker Deep Red” for 20 min at 37 °C. Colocalization was assessed by the Pearson correlation coefficient. Analysis was done using ImageJ software and the appropriate JACoP plugin [27].

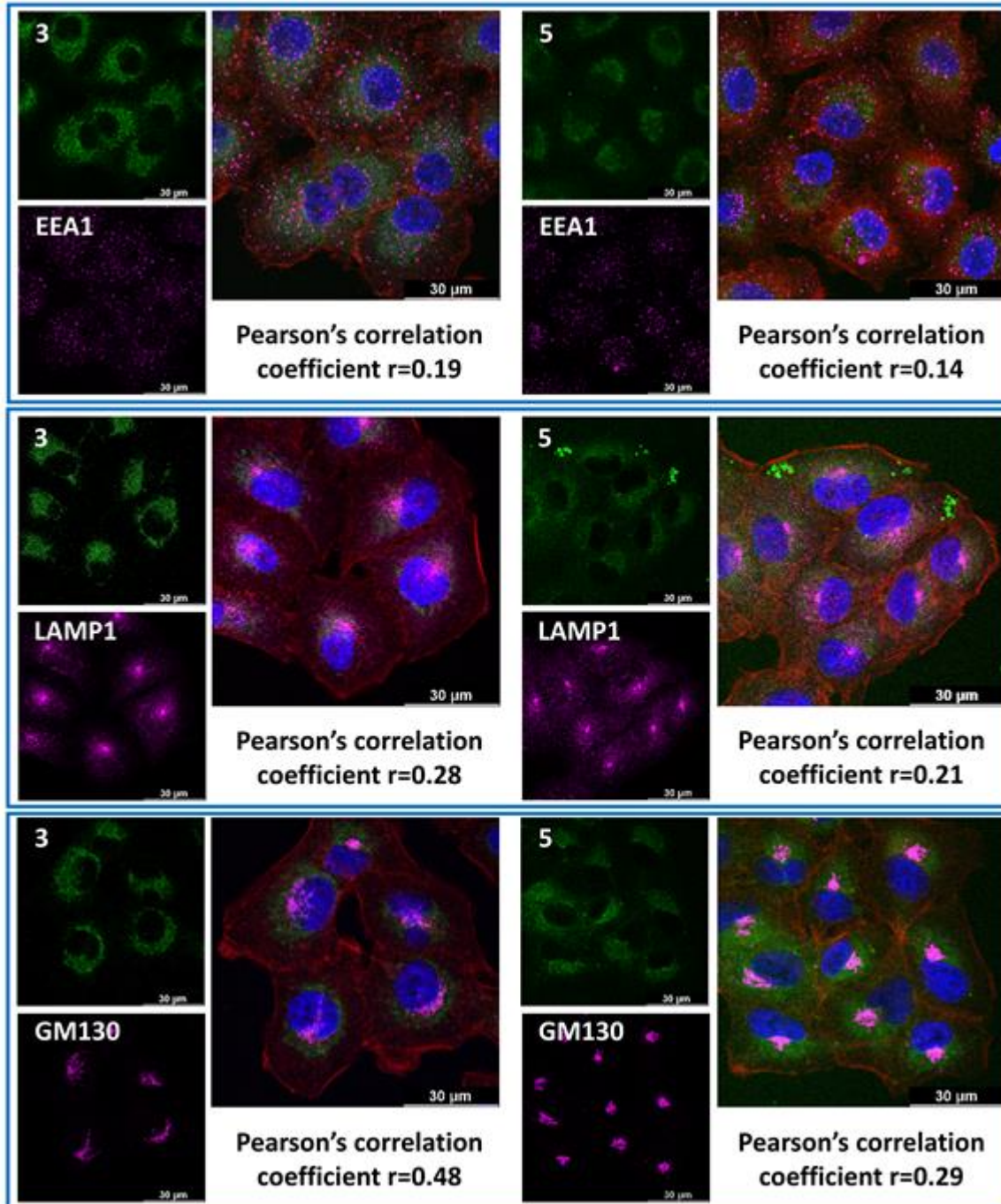


Figure 7. Intracellular localization of compounds **3** and **5** in A549 cells. Colocalization of compound **3** or **5** with early endosomes (EEA1), Golgi (GM130) or lysosomes (LAMP1) observed by confocal microscopy. Cells were treated with 10 μM of compound for 90 min at 37 $^{\circ}\text{C}$. Nuclei were stained with DAPI, in blue. Actin filaments were labelled with phalloidin, in red. Colocalization was assessed by the Pearson correlation coefficient. Analysis was done using ImageJ software and the appropriate JACoP plugin.

In further confocal microscope experiments, we collected the emission spectrum of a cluster of cytoplasmic organelles stained by **5** and compared it with the emission spectrum of the free dye in a buffered solution collected at different aggregation states [16] (Figure 8). As reported previously [16], at room temperature **5** is strongly aggregated with a characteristic emission at 600 nm, whereas at high temperature, it de-aggregates, emitting at 500 nm. The emission spectrum in the cell matched that of the non-aggregated form nicely, supporting the presence of single molecules of **5** bound to the cellular target.

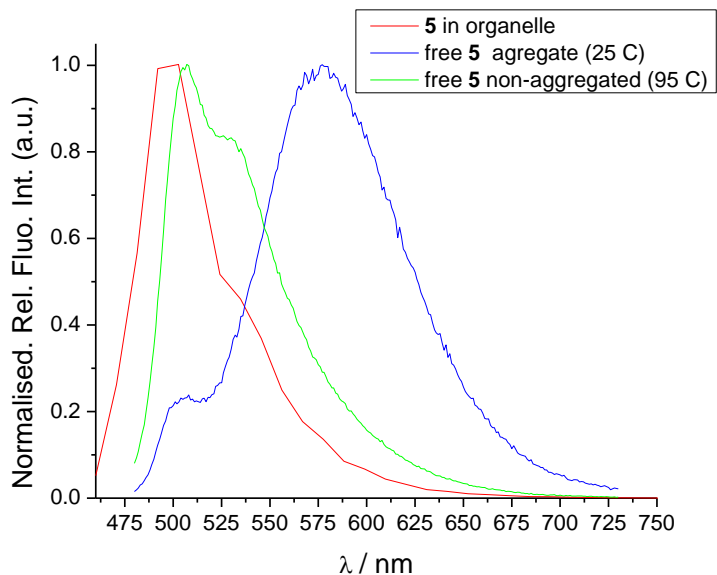


Figure 8. Fluorescence spectra of **5**: blue (at 25 °C) and green (at 95 °C) line ($c(\mathbf{5}) = 5 \times 10^{-7}$ M, $\lambda_{\text{exc}} = 470$ nm, pH 7.0, $I = 0.05$ M in sodium cacodylate buffer; red line ($c(\mathbf{5}) = 1 \times 10^{-5}$ M, $\lambda_{\text{exc}} = 457$ nm, pH 7.4, inside A549 cell organelle, as shown on Figure 8).

Light-irradiated compounds **3** and **5** show anti-adenovirus activity

A) Fluorimetric titrations with adenovirus

Human adenovirus type **5** (HAdV5) is a non-enveloped double-stranded DNA virus with an icosahedral protein capsid [42] often used as a vector in numerous clinical trials, particularly in cancer gene therapy [43]. The infectivity of HAdV5 depends on the binding of viral capsid proteins to receptors on the cell surface, followed by internalization, intracellular trafficking, and delivery of the genome to the nucleus. In all of these steps, surface exposed capsid proteins play a role, so prevention of their function can lead to unsuccessful infection, i.e., prevention of genome delivery and production of progeny virions [44].

Previously, we reported that triarylborane-containing compounds show binding to proteins characterized by strong changes in triarylborane fluorescence; [22,45] thus, we expected to observe similar fluorimetric responses with compounds **3** and **5** when titrated with HAdV5. Due to precautions when handling viral material, only a limited set of additions in fluorimetric titrations was possible; however, strong changes in the emission of **3** or **5** were observed (Figure 8).

The emission of **3** was quenched at a low viral concentration, but further addition of virus yielded a strong emission increase and hypsochromic shift of the maximum (Figure 8, left), the latter change closely resembling changes observed previously for the bithiophene analogue bound to BSA [22]. Such opposite changes suggest two different binding sites for **3** on HAdV5 particles, dependent on the **3**/virus ratio in solution.

At variance to **3**, addition of HAdV5 to anthracene-analogue **5** yielded only its emission quenching (Figure 8, right), ending with dominant maximum at about 580 nm, characteristic of anthracene aggregates [16]. Nonlinear fitting of the titration data to the 1st exponential equation (Figure 8, bottom) supported the formation of one dominant type of non-covalent **5**/HAdV5 complex. However, due to the huge difference in size of **5** (12 Å) and HAdV5 (700-1000 Å), it is likely that more molecules of **5** are bound to the homologous binding sites of a single virus particle, thus hampering accurate determination of the stoichiometry of the **5**/HAdV5 complex and determination of the corresponding binding constant. Nevertheless, titration ended at a very low concentration of virus in solution (1.5×10^{12} virus particles/mL), suggesting a very high affinity.

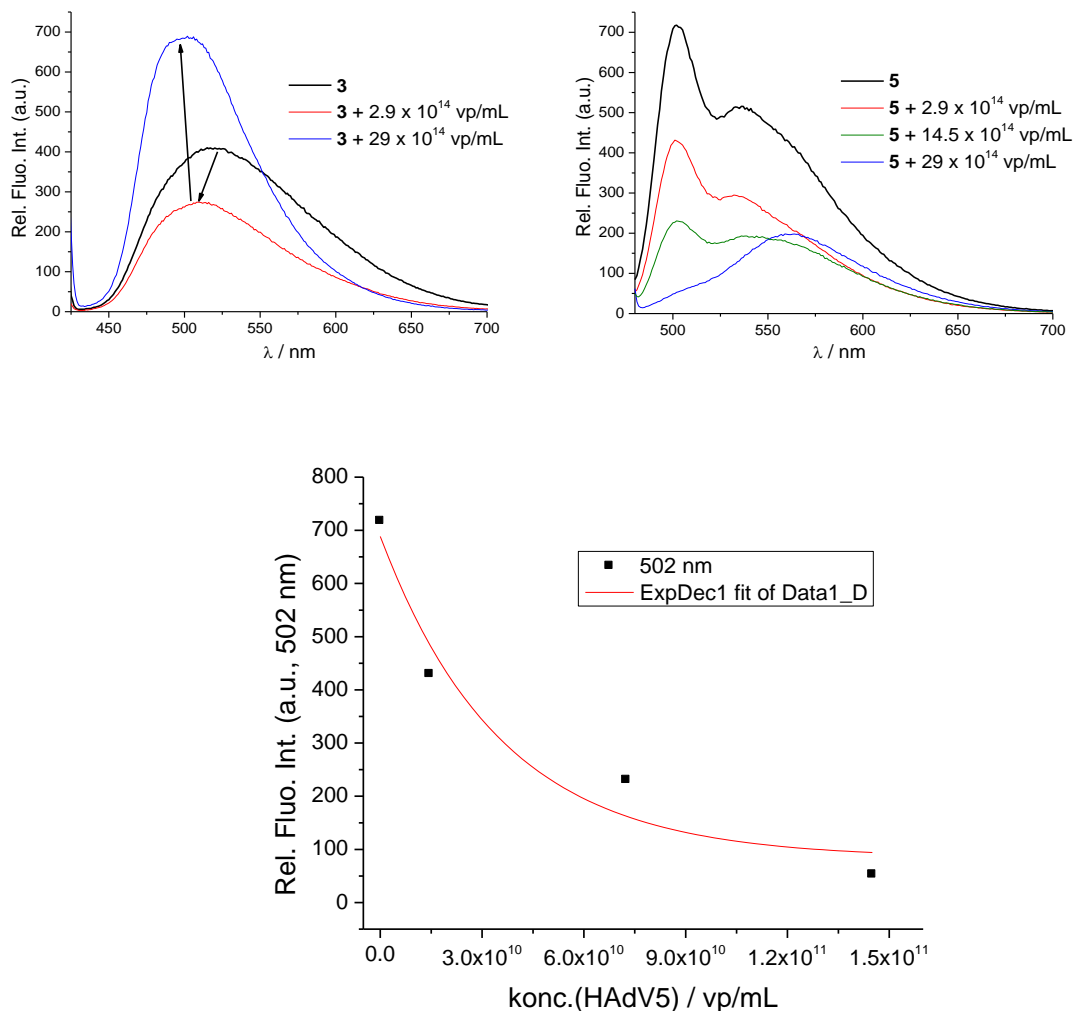


Figure 9. Change in the fluorescence spectra of: (Left) **3** ($c(\mathbf{3}) = 5.0 \times 10^{-7}$ M, $\lambda_{\text{exc}} = 412$ nm) and (RIGHT) **5**, ($c(\mathbf{5}) = 5.0 \times 10^{-7}$ M, $\lambda_{\text{exc}} = 470$ nm) upon addition of with human adenovirus type 5 ($c_{\text{stock}}(\text{HAdV5}) = 2.90 \times 10^{12}$ virus particles (vp)/mL). Done at pH = 7.0, Na cacodylate buffer, $I = 0.05$ M. Bottom: change of emission from **5** at 502 nm as a function of $c(\text{HAdV5})$ and fit to a 1st exponential (red line), supporting the formation of a noncovalent **5**/ HAdV5 complex.

*B) End-point dilution assay: UV-light irradiated compounds **3** and **5** exhibit anti-viral activity*

The impact of compounds **3** and **5** on HAdV5 infectivity was assessed by an end-point dilution assay. Prior to infecting the cells, virus suspension in $c(\mathbf{3}$ or $\mathbf{5}) = 5 \times 10^{-6}$ M solution was irradiated with visible light (Wolfram bulb light, 100W) for 10, 20, and 40 min, causing **3** or **5**-induced singlet oxygen formation and consequently damage to viral proteins. As

shown in Figure 10, light irradiation of chromophores **3** and **5** significantly decreased the titre of HAdV5 i.e., number of infective viruses (IU/mL). The antiviral activity of compound **5** is more pronounced than that of **3**. Irradiation of compound **5**-treated virus for 40 min decreased the HAdV5 titre for more than 80%, compared to a reference experiment with only the virus exposed to light. However, even in the dark, **5** decreased the HAdV5 titre by 25% in comparison to non-treated virus (data not shown), while, in the dark, **3** did not show anti-adenovirus activity. Thus, compound **5** exhibits better antiviral activity than compound **3**, probably due to a single mode of binding to the virus and consequently more effective light-induced protein damage.

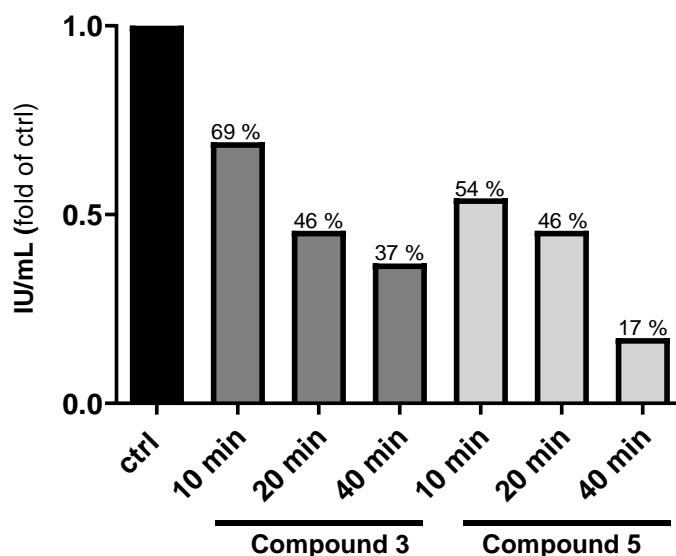


Figure 10. Antiviral activity of compounds **3** and **5** against HAdV5 in HEK-293 cells. Data are presented as IU/mL relative to the control sample (ctrl; viruses incubated in culture medium with light irradiation for 40 min). Representative data from three independent experiments which yielded similar results are shown.

4. Conclusions

This study showed that a recently reported class of low molecular weight fluorimetric / Raman-SERS sensors,[16] namely compounds **3** and **5**, exhibited rather efficient singlet oxygen production, as well as promising 2PA properties allowing their excitation by NIR irradiation. Compounds **3** and **5** very efficiently entered living human cells with negligible toxic effects, accumulating more or less non-selectively in various cytoplasmic organelles. Intriguingly, addition of compounds at 10 μ M concentration induced some ROS production in human cells, although with no extensive cytotoxic effect.

Only upon irradiation with visible light of the bio-applicable range (400 - 700 nm) **3** and **5** showed instantaneous (within 1-2 min) and very strong biological activity on human cell line, whereby significant change was related to the enhanced ROS production. Similar photo-toxic effect was observed toward HAdV5 virus, diminishing viral infectivity by order of magnitude.

Thus, compounds **3** and **5** were shown to serve as promising photosensitisers for PDT even with single-photo excitation (visible light range about 400-600 nm); however, they also have large 2PA cross-sections (350 and 390 GM at 770 nm, respectively), thus allowing their excitation in NIR range. They also strongly fluoresce in various cellular organelles, thus acting as theranostic agents for tumor- and virus-targeted photodynamic therapy. Obtained results strongly support further studies of **3** and **5** and their new analogues (currently being designed and synthesized) *in vivo* to characterize in detail their pharmacokinetic effects in living organisms.

Acknowledgements: The financial support of the Croatian Science Foundation project IP-2018-01-5475 and HRZZ-IP-2019-04-6048, the DAAD, and the Julius-Maximilians-Universität Würzburg are gratefully acknowledged.

References

- [1] G.M.F. Calixto, J. Bernegossi, L.M. De Freitas, C.R. Fontana, M. Chorilli, Nanotechnology-Based Drug Delivery Systems for Photodynamic Therapy of Cancer: A Review, *Molecules* 21 (2016) 342. <https://doi.org/10.3390/molecules21030342>
- [2] A.P. Castano, T.N. Demidova, M.R. Hamblin, Mechanisms in photodynamic therapy: part one - photosensitizers, photochemistry and cellular localization, *Photodiagnosis Photodyn. Ther.* 1 (2004) 279–93. doi: 10.1016/S1572-1000(05)00007-4
- [3] K. Plaetzer, B. Krammer, J. Berlanda, F. Berr, T. Kiesslich, Photophysics and photochemistry of photodynamic therapy: fundamental aspects, *Lasers Med Sci.* 24 (2009) 259–68. doi: 10.1007/s10103-008-0539-1
- [4] J.C.S. Simões, S. Sarpaki, P. Papadimitroulas, B. Therrien, G. Loudos, Conjugated Photosensitizers for Imaging and PDT in Cancer Research, *J. Med Chem.* 63 (2020) 14119–50. doi: 10.1021/acs.jmedchem.0c00047
- [5] A.P. Castano, T.N. Demidova, M.R. Hamblin, Mechanisms in photodynamic therapy: Part three - Photosensitizer pharmacokinetics, biodistribution, tumor localization and modes of tumor destruction, *Photodiagnosis Photodyn. Ther.* 2 (2005) 91–106. doi: 10.1016/S1572-1000(05)00060-8

[6] K. Ogawa, Y. Kobuke, Two-Photon Photodynamic Therapy by Water-Soluble Self-Assembled Conjugated Porphyrins, *BioMed Res Int.* 2013 (2013) 125658. <https://doi.org/10.1155/2013/125658>

[7] Z. Huang, A Review of Progress in Clinical Photodynamic Therapy, *Technol Cancer Res Treat* 4 (2005) 283–93. <https://doi.org/10.1177/153303460500400308>

[8] A. Mitra, G.I. Stables, Topical photodynamic therapy for non-cancerous skin conditions, *Photodiagnosis Photodyn. Ther.* 3 (2006) 116–27. doi: 10.1016/S1572-1000(06)00035-4

[9] A.F. dos Santos, G.S. Arini, D.R.Q. de Almeida, L. Labriola, Nanophotosensitizers for cancer therapy: a promising technology? *J. Phys. Mater.* 4 (2021) 032006. <https://doi.org/10.1088/2515-7639/abf7dd>

[10] A. Barбора, O. Bohar, A.A. Sivan, E. Magory, A. Nause, R. Minnes, Higher pulse frequency of near-infrared laser irradiation increases penetration depth for novel biomedical applications, *PLoS ONE* 16 (2021) 0245350. <https://doi.org/10.1371/journal.pone.0245350>

[11] E. Michail, Design and Development of a Two-Photon Absorption Induced Fluorescence Spectrometer and the Investigation of Nonlinear Optical Properties of Organic Chromophores [Internet], Universität Würzburg, (2021) [cited 2021 Nov 24]. <https://opus.bibliothek.uni-wuerzburg.de/frontdoor/index/index/docId/24218>

[12] X.-Q. Xu, Y. He, Y. Wang, Near-infrared organic chromophores with *pH*-sensitive, non-radiative emission for intelligent disease treatment, *Cell Rep Phys Sci.* 2 (2021) 100433. <https://doi.org/10.1016/j.xcrp.2021.100433>

[13] F. Bolze, S. Jenni, A. Sour, V. Heitz, Molecular photosensitisers for two-photon photodynamic therapy, *Chem. Commun.* 53 (2017) 12857–77. <https://doi.org/10.1039/C7CC06133A>

[14] M. Rumi, J.W. Perry, Two-photon absorption: an overview of measurements and principles, *Adv. Opt. Photonics* 2 (2010) 451–518. <https://doi.org/10.1364/AOP.2.000451>

[15] S.M. Berger, T.B. Marder, Applications of Triarylborane Materials in Cell Imaging and Sensing of Bio-relevant Molecules such as DNA, RNA, and Proteins, *Mater. Horiz.* 9 (2022) 112-120. <https://doi.org/10.1039/D1MH00696G>

L. Ji, S. Griesbeck, T.B. Marder, Recent Developments in and Perspectives on Three-Coordinate Boron Materials: A Bright Future, *Chem. Sci.* 8 (2017) 846-863. <https://doi.org/10.1039/C6SC04245G>

C.D. Entwistle, T.B. Marder, Applications of Three-Coordinate Organoboron Compounds and Polymers in Optoelectronics, Special Issue on Organic Electronics, *Chem. Mater.* 16 (2004) 4574-4585. doi:10.1021/CM0495717

C.D. Entwistle, T.B. Marder, Boron Chemistry Lights the Way: Optical Properties of Molecular and Polymeric Systems, *Angew. Chem. Int. Ed. Engl.* 41 (2002) 2927-2931; *Angew. Chem.* 114 (2002) 3051-3056. doi: 10.1002/1521-3773(20020816)41:16<2927::AID-ANIE2927>3.0.CO;2-L

[16] M. Ferger, Ž. Ban, I. Krošl, S. Tomić, L. Dietrich, S. Lorenzen et al. Bis(phenylethynyl)arene Linkers in Tetracationic Bis-triarylborane Chromophores Control Fluorimetric and Raman Sensing of Various DNAs and RNAs, *Chem. Eur. J.* 27 (2021) 5142–5159. doi: 10.1002/chem.202005141

[17] W. T. Wu, X. D. Shao, J. Z. Zhao, M. B. Wu, Controllable Photodynamic Therapy Implemented by Regulating Singlet Oxygen Efficiency, *Adv. Sci.* 4 (2017) 1700113. doi: 10.1002/adv.201700113

[18] G. Shi, S. Monro, R. Hennigar, J. Colpitts, J. Fong, K. Kasimova, H.M. Yin, R. DeCoste, C. Spencer, L. Chamberlain, A. Mandel, L. Lilge, S.A. McFarland, Ru(II) dyads derived from alpha-oligothiophenes: A new class of potent and versatile photosensitizers for PDT, *Coord. Chem. Rev.* 282 (2015) 127-138. <https://dx.doi.org/10.1016/j.ccr.2014.04.012>

[19] S. Griesbeck, Z.L. Zhang, M. Gutmann, T. Luhmann, R.M. Edkins, G. Clermont, A. N. Lazar, M. Haehnel, K. Edkins, A. Eichhorn, M. Blanchard-Desce, L. Meinel, T.B. Marder, Water-Soluble Triarylborane Chromophores for One- and Two-Photon Excited Fluorescence Imaging of Mitochondria in Cells, *Chem. Eur. J.* 22 (2016) 14701-14706. <https://doi.org/10.1002/chem.201602639>

[20] S.M. Berger, J. Ruhe, J. Schwarzmann, A. Phillipps, A.K. Richard, M. Ferger, I. Krummenacher, L. M. Tumir, Z. Ban, I. Crnolatac, D. Majhen, I. Barisic, I. Piantanida, D. Schleier, S. Griesbeck, A. Friedrich, H. Braunschweig, T.B. Marder, Bithiophene-Cored, mono-, bis-, and tris-(Trimethylammonium)-Substituted, bis-Triarylborane Chromophores: Effect of the Number and Position of Charges on Cell Imaging and DNA/RNA Sensing, *Chem. Eur. J.* 27 (2021) 14057-14072. doi: 10.1002/chem.202102308

[21] S. Griesbeck, E. Michail, F. Rauch, H. Ogasawara, C. Wang, Y. Sato, R. Edkins, Z. Zhang, M. Taki, C. Lambert, S. Yamaguchi, T.B. Marder, The Effect of Branching on One- and Two-Photon Absorption, Cell Viability and Localization of Cationic Triarylborane Chromophores with Dipolar vs. Octupolar Charge Distributions for Cellular Imaging, *Chem. Eur. J.* 25 (2019) 13164-13175. doi: 10.1002/chem.201902461.

S. Griesbeck, E. Michail, C. Wang, H. Ogasawara, S. Lorenzen, L. Gerstner, T. Zhang, J. Nitsch, Y. Sato, R. Bertermann, M. Taki, C. Lambert, S. Yamaguchi, T.B. Marder, Tuning the π -Bridge of Quadrupolar Triarylborane Chromophores for One- and Two-Photon Excited Fluorescence Imaging of Lysosomes in Live Cells, *Chem. Sci.* 10 (2019) 5405-5422. <https://doi.org/10.1039/c9sc00793h>

S. Griesbeck, M. Ferger, C. Czernetzi, C. Wang, R. Bertermann, A. Friedrich, M. Haehnel, D. Sieh, M. Taki, S. Yamaguchi, T.B. Marder, Optimization of Aqueous Stability versus π -Conjugation in Tetracationic Bis(triarylborane) Chromophores: Applications in Live-Cell Imaging,” *Chem. Eur. J.* 25 (2019) 7679-7688. doi: 10.1002/chem.201900723.

S.M. Berger, T.B. Marder, Applications of Triarylborane Materials in Cell Imaging and Sensing of Bio-relevant Molecules such as DNA, RNA, and Proteins, *Mater. Horiz.* 9 (2022) 112-120. <https://doi.org/10.1039/D1MH00696G>

[22] Z. Ban, S. Griesbeck, S. Tomic, J. Nitsch, , T.B. Marder, I. Piantanida, A Quadrupolar Bis-Triarylborane Chromophore as a Fluorimetric and Chiroptic Probe for Simultaneous and Selective Sensing of DNA, RNA and Proteins, *Chem. Eur. J.* 26 (2020) 2195-2203. <https://doi.org/10.1002/chem.201903936>

[23] H. Amini, Z. Ban, M. Ferger, S. Lorenzen, F. Rauch, A. Friedrich et al., Tetracationic Bis-Triarylborane 1,3-Butadiyne as a Combined Fluorimetric and Raman Probe for Simultaneous and Selective Sensing of Various DNA, RNA and Proteins, *Chem. Eur. J.* 26 (2020) 6017–28. <https://doi.org/10.1002/chem.201905328>

[24] N.S. Makarov, M. Drobizhev, A. Rebane, Two-photon absorption standards in the 550–1600 nm excitation wavelength range, *Opt Express.* 16 (2008) 4029–47. <https://doi.org/10.1364/OE.16.004029>

[25] S. de Reguardati, J . Pahapill, A. Mikhailov, Y. Stepanenko, A. Rebane, High-accuracy reference standards for two-photon absorption in the 680-1050 nm wavelength range, *Opt. Express* 24 (2016) 9053–66. <https://doi.org/10.1364/OE.24.009053>

[26] G. Radcliff, M. J. Jaroszeski, Basics of flow cytometry, *Methods Mol. Biol.* 91 (1998) 1-24. doi: 10.1385/0-89603-354-6:1.

[27] S. Bolte, F.P. Cordelières, A guided tour into subcellular colocalization analysis in light microscopy, *J. Microsc.* 224 (2006) 213–32. doi: 10.1111/j.1365-2818.2006.01706.x

[28] L.J. Reed, H. Muench, A simple method of estimating fifty percent endpoints 12. *Am. J. Epidemiol.* 27 (1938) 493–7. <https://doi.org/10.1093/oxfordjournals.aje.a118408>

[29] P.R. Ogilby, Singlet oxygen: there is indeed something new under the sun, *Chem. Soc. Rev.* 39 (2010) 3181-3209. <https://doi.org/10.1039/B926014P>

[30] R. Schmidt, C. Tanielian, R. Dunsbach, C. Wolff, Phenalenone, a universal reference compound for the determination of quantum yields of singlet oxygen O₂(¹Δ_g) sensitization,

J. Photochem. Photobiol. A 79 (1994) 11-17. [https://doi.org/10.1016/1010-6030\(93\)03746-4](https://doi.org/10.1016/1010-6030(93)03746-4)

[31] see Table S2 in Supporting Information of M. Bregnhøj, M. Westberg, B.F. Minaev, P.R. Ogilby, Singlet Oxygen Photophysics in Liquid Solvents: Converging on a Unified Picture, Acc. Chem. Res. 50 (2017) 1920-1927. <https://doi.org/10.1021/acs.accounts.7b00169>

[32] B. A. Coombs, S. R. Rutter, A. E. Goeta, H. A. Sparkes, A. S. Batsanov, A. Beeby, 2,5-bis(Arylethynyl)thienyl systems: Preparation and photophysical properties. Part II, RSC Adv. 2 (2012) 1870–1876. <https://doi.org/10.1039/C1RA00728A>

[33] J.D. Bhawalkar, N.D. Kumar, C.-F. Zhao, P.N. Prasad, Two-Photon Photodynamic Therapy, J Clin Laser Med. Surg. 15 (1997) 201–4. doi: 10.1089/clm.1997.15.201

[34] R.L. Goyan, D.T. Cramb, Near-infrared two-photon excitation of protoporphyrin IX: photodynamics and photoproduct generation, Photochem. Photobiol. 72 (2000) 821–7. doi: 10.1562/0031-8655(2000)072<0821:nitpeo>2.0.co;2

[35] P. Gierlich, S.G. Mucha, E. Robbins, L. C. Gomes-da-Silva, K. Matczyszyn, M.O. Senge, One-Photon and Two-Photon Photophysical Properties of Tetrafunctionalized 5,10,15,20-tetrakis(m-hydroxyphenyl)chlorin (Temoporfin) Derivatives as Potential Two-Photon-Induced Photodynamic Therapy Agents, Chemphotochem (2022) e202100249. <https://doi.org/10.1002/cptc.202100249>

[36] C.L. Sun, Q. Liao, T. Li, J. Li, J.Q. Jiang, Z.Z. Xu, X. D. Wang, R. Shen, D.C. Bai, Q. Wang, S.X. Zhang, H.B. Fu, H.L. Zhang, Rational design of small indolic squaraine dyes with large two-photon absorption cross section, Chem. Sci. 6 (2015) 761-769. <https://doi.org/10.1039/C4SC02165G>

[37] A. Dobos, W. Steiger, D. Theiner, P. Gruber, M. Lunzer, J. Van Hoorick, S. Van Vlierberghe, A. Ovsianikov, Screening of two-photon activated photodynamic therapy sensitizers using a 3D osteosarcoma model, Analyst 144 (2019) 3056-3063. <https://doi.org/10.1039/C9AN00068B>

[38] a) Z.Y. Sun, L.P. Zhang, F.P. Wu, Y.X. Zhao, Photosensitizers for Two-Photon Excited Photodynamic Therapy, Adv. Funct. Mater. 27 (2017) 1704079. <https://doi.org/10.1002/adfm.201704079>; b) , F. Bolze, S. Jenni, A. Sour, V. Heitz, Molecular photosensitisers for two-photon photodynamic therapy, Chem. Commun. 53 (2017) 12857-12877. <https://doi.org/10.1039/C7CC06133A>; c) L.K. McKenzie, H.E. Bryant, J. A. Weinstein, Transition metal complexes as photosensitisers in one- and two-photon photodynamic therapy, Coordin. Chem. Rev. 379 (2019) 2-29. <https://doi.org/10.1016/j.ccr.2018.03.020>

[39] F. Heinemann, J. Karges, G. Gasser, Critical Overview of the Use of Ru(II) Polypyridyl Complexes as Photosensitizers in One-Photon and Two-Photon

Photodynamic Therapy, *Accounts. Chem. Res.* 50 (2017) 2727-2736. doi: 10.1021/acs.accounts.7b00180

[40] C.Q. Tang, P. Hu, E. Ma, M.D. Huang, Q.D. Zheng, Heavy atom enhanced generation of singlet oxygen in novel indenofluorene-based two-photon absorbing chromophores for photodynamic therapy, *Dyes Pigments* 117 (2015) 7-15. <https://doi.org/10.1016/j.dyepig.2015.01.019>

[41] T. V. Esipova, H. J. Rivera-Jacquez, B. Weber, A. E. Masunov, S. A. Vinogradov, Two-Photon Absorbing Phosphorescent Metalloporphyrins: Effects of pi-Extension and Peripheral Substitution, *J. Am. Chem. Soc.* 138 (2016) 15648-15662. <https://doi.org/10.1021/jacs.6b09157>

[42] J. Gallardo, M. Pérez-Illana, N. Martín-González, C. San Martín, Adenovirus Structure: What Is New? *Int. J. Mol. Sci.* 22 (2021) 5240. <https://doi.org/10.3390/ijms22105240>

[43] T.G. Cunliffe, E.A. Bates, A.L. Parker, Hitting the Target but Missing the Point: Recent Progress towards Adenovirus-Based Precision Virotherapies, *Cancers* 12 (2020) 3327. <https://doi.org/10.3390/cancers12113327>

[44] D. Nestić, K. Božinović, I. Pehar, R. Wallace, A.L. Parker, D. Majhen, The Revolving Door of Adenovirus Cell Entry: Not All Pathways Are Equal, *Pharmaceutics* 13 (2021) 1585. <https://doi.org/10.3390/pharmaceutics13101585>